*Journal of Machine Engineering, 2026, Vol. 26*
*ISSN 1895-7595 (Print)  ISSN 2391-8071 (Online)*

Received*: 09 March 2026* / Accepted: *04 May 2026* / Published online: *02 June 2026*

*heat treatment,*
*mechanical properties,*
*fatigue test,*
*impact test*

Hadi Raheem IBRAHIM[1*],
Rabea Sami JOODI[1],
Ali Hameed Mohammed SAEED[1]

# EXPERIMENTAL AND PREDICTIVE INVESTIGATION OF FATIGUE RESISTANCE IN HEAT-TREATED AISI 1045 STEEL UNDER WATER AND OIL QUENCHING CONDITIONS

This research paper examines the impact of post-review cooling on the fatigue resistance of medium carbon steel (AISI 1045 S45C) through the application of various heat treatments and quenching in water or oil at temperatures of 275Co, 475Co and 675Co. It also compares the effects of the two quenching media on the mechanical properties and fatigue resistance of the steel. Fatigue tests were performed under steady stress conditions with a stress ratio of -1. The results of the experiments indicate that water quenching at a holding temperature of 275Co for one hour provides the greatest fatigue resistance for the steel. This is due to the formation of diluted martensite. Long fatigue cracks were accurately measured using a scanning electron microscope (SEM). Two models were selected to evaluate the fatigue life of AISI 1045 S45C medium carbon steel tempered and hardened at different cooling temperatures. The first model was selected from the crack growth rate equation (dE/dN), and the second from the stress intensity factor equation (ΔS).

## 1. INTRODUCTION

The key to manufacturing any mechanical product that is acceptable to both the industrial sector and consumers lies in ensuring that its cost remains within reasonable economic limits, thereby guaranteeing its marketability and usability. To accomplish this goal in metal cutting or machining operations, numerous attempts have been made using various methods, such as improving tool life to reduce production costs, maximizing production rates to lower costs, and so on. However, no effort has been completely successful due to the many complexities involved in the process. For example, if the cutting speed is reduced to increase tool life, the metal removal rate will also decrease, and thus, the production cost will increase. A similar effect is observed if efforts are made to increase tool life by reducing the feed rate

[1] Al-Mussaib Technical Institute, Al-Furat Al-Awsat Technical University, 51009 Babylon, Iraq
[*] E-mail: inm.hadi@atu.edu.iq
https://doi.org/10.36897/jme/221402

and cutting depth. Conversely, if efforts are made to increase the production rate or reducing cutting time by increasing cutting speed, feed rate, and cutting depth clearly shortens tool life, thereby increasing operating costs and, consequently, the total cost of cutting and production. Therefore, it is necessary to strike a balance and determine an appropriate cutting speed that ensures economical tool life and produces economic output. This research paper illustrates one such method for improving the production rate in various metal cutting operations [1, 2].

Increasing global competition, environmental changes, and increasingly complex supply chains are driving companies to seek more effective solutions that meet customer needs and requirements. The development of information and communication technology can contribute to meeting these challenges. Automation and industrial robotics in production are attracting increasing attention from scientists and practitioners. The article reviews the status of selected manufacturing companies in terms of their readiness and level of interest in implementing solutions that automate manufacturing processes [3].

Another research paper leads to the conclusion that the cooling rate has a significant effect on the mechanical properties of steel 35. Samples were prepared for hardness, impact, tensile, and torsion tests. Several thermally treated samples were treated at a temperature of 850°C for one hour, then cooled using three different cooling environments (water, air, and furnace) were used to determine the effect of the appropriate cooling rate on the mechanical 6 properties. Microscopic examination was performed on all samples before and after treatment in a double thermal oven using a light microscope. To determine the develops resulting after being heat tackling and their influence on mechanical peculiarities, the practical results showed whose the steel microstructure it could be significantly mutation and amended by changing the cooling rate of the line, and therefore improving one property will affect the other properties due to the bonding between all peculiarities. In the aquatic environment, tensile strength, torsional strength, and stiffness exhibited noticeable increases, whereas impact resistance showed a decline. The air medium contributed to the enhancement of most mechanical properties, which can be attributed to the improved homogeneity of grain size distribution. In contrast, exposure to the furnace atmosphere resulted in enhanced ductility and impact strength [4, 5].

Different mechanical heat treatments were performed on high-strength low-carbon steel with a new chemical composition. As a result, three different microstructures with different mechanical properties and corrosion resistance were produced. Then, a heating heat treatment was performed to redistribute the phases in the steel. Microstructure “A”, containing 57% martensitic and 31% bainite, exhibited high strength and medium hardness, while microstructure “C”, containing 94% ferrite and 4% martensite/austenite, exhibited low strength and high hardness. Meanwhile, microstructure “B”, containing 97% bainite and 3% martensite/austenite, exhibited high strength and toughness. In contrast, corrosion generated by polarization curves in 0.11 molar H2SO4, 3.5 molar H2SO4, 3.6 wtpct NaCl, and NS4 solutions showed approximately similar volumes [6].

Four grades of API X60 stress-resistant steel pipes were produced by controlling the carbon and silicon content, with the aim of studying their effect on stress corrosion cracking (SCC). The results showed that steel containing 0.05% carbon by weight consists mainly of polygonal ferrite (PF), while steel containing 0.08% carbon consists of acicular ferrite (AF). It was also found that the proportion of acicular ferrite increases with increasing carbon

content, due to carbon's role as an austenite stabilizer. As for the effect of silicon, it was observed that steel containing 0.15% silicon has a higher volume fraction of bainitic ferrite compared to steel containing 0.25% silicon, while the fraction of secondary phases is lower.

Based on the mechanical properties of API X60 pipe steel before and after stress aging, an increase in yield stress and a decrease in both specific and total elongation were observed, a phenomenon known as the stress-aging effect. It was also found that this effect decreases in stress-relieved steel as the proportion of needle-like ferrite increases and the homogeneity of the secondary phase distribution improves. On the other hand, an excessive increase in carbon content leads to the formation of fine precipitates, where the stress-aging effect arises as a result of the interaction between dislocations and these fine precipitates. [7].

The lack of scanted regulations for enhancing the safety of skeletal elements and their resistance to accidental loads such as impacts, explosions, and fires has strongly motivated researchers to fill this disceming interstice. This study examines one of the most common and widely used structural elements in building construction, focusing on its importance and role in achieving structural efficiency and durability, steel beams with large lattice vents (SBLWOs), was subjected to a numerical study under load of impact. Nonlinear finite element (NLFE) models were established using ABAQUS software and validated against experimental data available in scientific references. The nonlinear finite element models were developed taking into state the dynamic properties of materials in the elastic, plastic, and damage phases. The effect of strain rate was also taken into account in the models. Subsequently, extensive parametric analyses were performed on the parameters affecting the behaviour of steel beams with large lattice openings, including impact energy, impact location, and opening reinforcement.

Compared results from the nonlinear finite element models and experimental tests showed remarkable agreement in terms of force data, time history, and failure modes. The results looked that SBLWOs were able to resist impact at a higher speed rather than with a larger mass. While the effect of the biasing location, the worst case was found to be when a cellular steel beam was impacted near the supports. Finally, incorporating steel struts along the impact path led to a substantial enhancement in the grid's resistance to shear forces and vibration. [8].

## 2. METHODOLOGY

### 2.1. MATERIALS

The metal is used in research is medium carbon steel (AISI 1045 S45C), Where it is used in industry for various industrial applications. Cylindrical rods of this metal, 6 m long and 19 mm in diameter, were obtained from Mechanical Industries General Company.

The chemical syntax of carbon medium steel (AISI 1045 S45C) was examined by performing chemical analysis using a spectrometer at the Specialized Institute for Engineering Industries. Table (1) shows the standard chemical composition and practical composition of the metal used in the current research paper.

Table 1. Chemical analysis results of the metal in paper

| Wt % | C | Si | Mn | P | S | Mo | Cu | Fe |
|---|---|---|---|---|---|---|---|---|
| Standard Value | 0.42-0.5 | 0.15-0.35 | 0.5-0.8 | ≤ 0.035 | ≤ 0.035 | - | - | Rem. |
| Actual Value | 0.465 | 0.223 | 0.578 | - | 0.031 | 0.079 | 0.017 | Rem. |

## 2.2. MANUFACTURING OF FATIGUE TEST SAMPLE

Standard specifications for testing on a rotating bending fatigue-testing machine. The received bars were cut into pieces with a length of 160 mm and a diameter of 20 mm, then surface grinding was performed using centre less grinding machines to obtain a final diameter of 10 mm. To obtain the curvature in the tow position as shown in Fig. 1 (R 35). The samples were run on a Harrison 600 reproduction lathe, where the sample was reproduced with the curvature found on a standard sample manufactured on a CNC machine, leaving a tolerance of 0.2 mm for manual smoothing and removal of deformations resulting from thermal treatments.

A conventional lathe was used to smooth the curved part (R 35) with silicon carbide smoothing sheets with degrees of smoothness of (125, 185, 225, 325, 400, 500, 600, 1000, and 1200) grit/cm2. Polishing was performed using 8/4 micron diamond paste with red polishing cloth and cooling fluids to achieve a high degree of smoothness and polish (Mirror Finishing).

Fig. 1. Standard specimen dimensions of fatigue test

The fatigue test samples were classified into five groups according to the type of heat treatment used, as shown in Table 2.

Table 2. Classification of fatigue test samples for medium carbon steel (AISI 1045 S45C)

| Type of heat treatment | Sample code | Group code |
|---|---|---|
| No interaction | - | a |
| Quenched in water at 850°C for 20 min.. | - | b |
| Hardening in water + review at 265°C for 60 min. | c1 | c |
| Quenching in water + review at 465°C for 60 min. | c2 | |
| Quenching in water + tempering at 675°C for 60 min. | c3 | |
| Hardening in oil at 850°C for 20 min | - | d |
| Hardening in oil + review at 265 oC for 60 min. | e1 | e |
| Hardening in oil + review at 465 oC for 60 min. | e2 | |
| Hardening in oil + review at 675°C for 60 min. | e3 | |

### 2.3. TENSILE TEST

A tensile test was performed on medium carbon steel (AISI 1045 S45C)), with one sample manufactured for each heat treatment in accordance with standard specification for tensile test samples, as shown in Fig 2. The tensile test was performed on a(SM1000 Universal Test Machine TeQuipment ) located at the Specialized Institute for Engineering Industries. Table 3 shows the results of the tensile test for medium carbon steel according to the type of heat treatment [9].

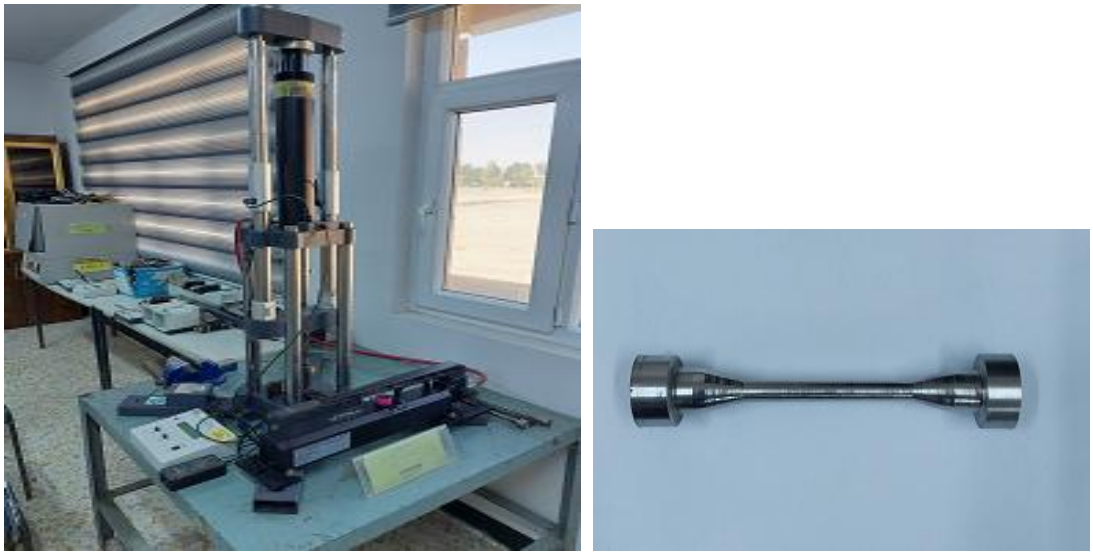

(a) (b)

Fig. 2. (a)The tensile test equipment, (b)The Tensile test sample

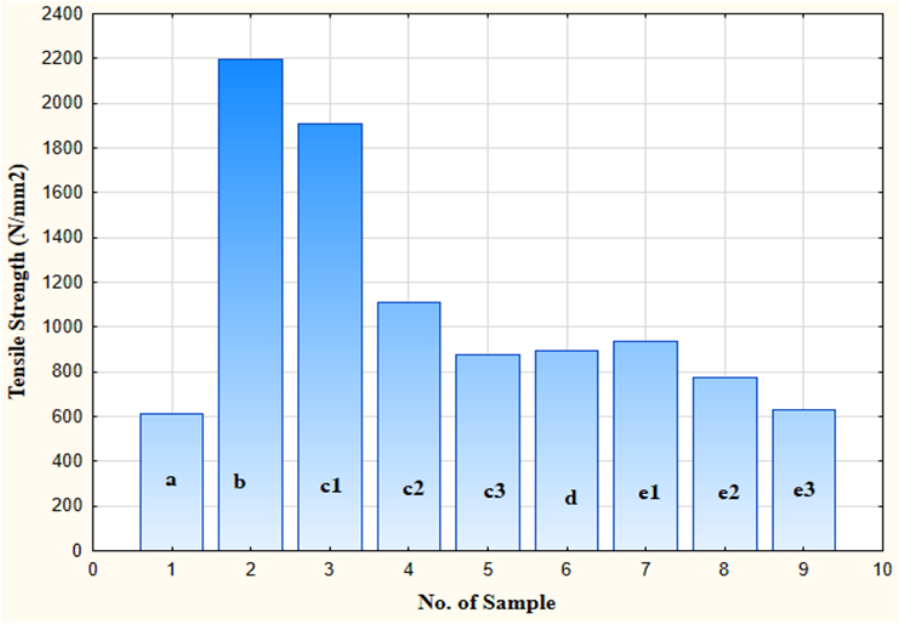


Fig. 3. Results of tensile test according the code of samples

2.4. MACRO HARDNESS TEST

First: The macro hardness test was performed using the Rockwell (HRC) method on a (Wilson / Rockwell Hardness Tester B524-R) located at the General Company for Electrical Industries for all treated and untreated samples. A diamond cone indenter with a load of 150 kg was used in the device, three readings were taken for each sample directly from the device, and the average of these readings was adopted. This test (i.e., Vickers hardness test) was conducted in the laboratory of mechanical department in Almusaib institute as shown in figure 4 and the results of this test are show in Table 4.


Fig. 4. Electronic hardness tester with indenter for Rockwell hardness testing

Table 3. Hardness test results for medium carbon steel according to heat treatment type

| Specimen | a | b | c1 | c2 | c3 | d | e1 | e2 | e3 |
|---|---|---|---|---|---|---|---|---|---|
| H.R.C | 17.5 | 58.9 | 48,8 | 35.3 | 24.7 | 26.5 | 28.6 | 22.5 | 17.9 |
| H.V. | 214 | 700 | 502 | 348 | 268 | 276 | 288 | 239 | 219 |

2.5. FATIGUE TESTING

The fatigue test used in this research is rotating bending fatigue, and the device used is a TERCO MT3012 Rotating Bending Machine located in the laboratory of material strength in mechanical department of Almusaib institute, as shown in Fig. 4.

Fig. 5. Fatigue testing device used in the current study

For smooth samples, fatigue tests were conducted with constant loads and a stress ratio ($R = -1$). This apparatus exposes the test piece's surface to alternating compressive and tensile stresses as it spins by applying a force perpendicular to the test piece's axis from the right side of the piece holder [10, 11].

A meter is included with the gadget to track the number of stress cycles at a 3000 rpm rotational speed. An iron block that moves on a 30-cm-long iron threshold is used to apply the stress. The movement of the block on the sill indicates the value of the bending stress based on the bending moment calculation. When it,

$$PF = \left(\frac{D}{6.75}\right)^{3} \tag{1}$$

$$Slide\ (cm) = \frac{Stress}{9.81} \tag{2}$$

The moment of the part that bends at the centre of the model and the stress generated on it.

$$M_b = \frac{G.L}{a}\,.b = \frac{1.5{*}L}{5} * 10 = 3L \tag{3}$$

$$\sigma = \frac{M_b}{W} = \frac{G.L{*}b}{a.W} = \frac{3.L}{0.003} = 100L \tag{4}$$

$$Where,\ \ W = \frac{I}{Y} \tag{5}$$

## 2.6. IMPACT TESTING

Impact testing was performed using the Charpy method on samples heat-treated under various conditions in accordance with the standard specifications for impact samples and charpy test equipment shown in Fig. 5. A BROOKSCharpy Impact Testing Machine (Mass Block-30Kg) located at the Almusaib technical institute laboratories were used. Both the impact energy and impact resistance were calculated practically as shown in Table 5, and the following law was used to calculate the impact resistance [12].

$$\sigma_{impact} = \frac{E}{A} = \frac{WL(cos\alpha_1 - cos\alpha_2)}{A} \tag{6}$$


(a) (b)

Fig. 6. (a) A BROOKS Charpy Impact Testing Machine, (b) Impact sample of charpy test

Table 4. Charpy impact test results

| No. | Specimen | $\alpha_1$ | E (J)Practically | Practically $\sigma_i$ (KJ/m2) |
|---|---|---|---|---|
| 1 | a | 132 | 23 | 272 |
| 2 | b | 133 | 21 | 245 |
| 3 | c1 | 132 | 23 | 272 |
| 4 | c2 | 111 | 76 | 943 |
| 5 | c3 | 100 | 108 | 1340 |
| 6 | d | 110 | 79 | 977 |
| 7 | e1 | 107 | 88 | 1083 |
| 8 | e2 | 109 | 82 | 1015 |
| 9 | e3 | 98 | 114 | 1415 |

## 3. RESULTS AND DISCUSSION

The model the life and impact of the fatigue stresses, water quenched after review at 275, 475, 675 °C, and repeated cracking and failure cycles for each sample, researchers reviewed the water samples and used these cracks' resulting in a mathematical model that predicted the life cycles of the pieces.

* A relationship was drawn between the length of the crack and the number of cycles for different stresses, and from this relationship, mathematical equations were found for each temperature, as shown in Tables (6), (7), and (8).

*Plot a relationship between the speed of incision and the intensity of stress from this relationship, mathematical equations were found for each reference temperature, which are:

$$\frac{de}{dN} = 0.0235 * 10^{-3} * (\Delta S^{-1.794}) \text{for Temp. } 275\ \text{C}^{\text{o}} \tag{7}$$

$$\frac{de}{dN} = 11.89 * (\Delta S^{-3.759}) \text{ for Temp. } 475\ \text{C}^{\text{o}} \tag{8}$$

$$\frac{de}{dN} = 0.0275 * 10^{-3} * (\Delta S^{-2.403}) \text{for Temp. } 675\ \text{C}^{\text{o}} \tag{9}$$

Substitution (ΔS) by $(K\ \Delta\sigma\sqrt{\pi e})$

Where $K$ is shape factor =1, then:

$$\frac{de}{dN} = 16.75 * 10^{-3} * \left(\sigma_f\right)^{-1.794} * a^{0.895} \text{for Temp. } 275\text{C}^{\text{o}} \tag{10}$$

$$\frac{de}{dN} = 2.75 * \left(\sigma_f\right)^{-3.759} * a^{1.88} \text{ for Temp. } 475\text{C}^{\text{o}} \tag{11}$$

$$\frac{de}{dN} = 13.83 * 10^{-3} * \left(\sigma_f\right)^{-2.403} * a^{-1.203} \text{for Temp. } 675\text{C}^{\text{o}} \tag{12}$$

Plot a relationship between the crack rate generation and the stress intensity factor for all temperatures and find the mathematical equation for the relationship, which is,

$$\frac{de}{dN} = 1.275 * 10^{-9} * \Delta S^{1.897} \tag{13}$$

Plot a relationship between stress intensity for all temperatures and the reference temperature ($T$) and find the mathematical equation for the relationship, which is,

$$\Delta S = 3005.9 * T^{-0.634} \tag{14}$$

Plot a graph showing the relationship between the crack rate generation for all temperatures and the reference temperature (T), and find the mathematical equation for this relationship, which is,

$$\frac{de}{dN} = 6.897 * 10^{-3} * T^{-1.255} \tag{15}$$

Equations (13) and (15) were equated, and after substituting ( ΔS) with ($K\Delta\sigma\sqrt{\pi e}$ ) in equation (14), the following was obtained,

$$e = \frac{907295}{\sigma_f^2 * T^{1.325}} \tag{16}$$

From the compensation for the integration of equation (15) (ΔS) in equation (14).

$$e = \frac{719255}{\sigma_f^2 * T^{1.325}} \tag{17}$$

$$e = 6.897 * 10^{-3} * T^{-1.255} * N \tag{18}$$

Equations (16) and (18) were equated, as were (17) and (18), to obtain two equations, each representing the age of the part:

$$N_f = \frac{0.198 * 10^9}{\sigma_f * T^{0.0698}} \tag{19}$$

$$N_f = \frac{99.97 * 10^9}{\sigma_f^2 * T^{0.0698}} \tag{20}$$

To solve the above equations numerically, the following mathematical formulas were used

$$e = b_o + b_1 N + b_2 * N^2 \tag{21}$$

$$\frac{de}{dN} = b_1 + b_2 * N \tag{22}$$

Table 5. Calculations for crack growth in water-quenched steel and references at (275°C)

| bo= -0.066 | b1= 9.33 x 10-6 | | b2 =1.52 x 10-11 | |
|---|---|---|---|---|
| a (mm) | Nf (cycle) | $\sigma$ (N/mm2) | de/dN (mm/cycle) | ΔS $(MPa.m^{1/2})$ |
| 0.97 | 1.42x105 | 832 | 7.232x10-6 | 45.52 |
| 0.99 | 1.56x105 | 822 | 7.015 x10-6 | 45.57 |
| 1.14 | 1.74x105 | 803 | 6.746 x10-6 | 47.47 |
| 1.23 | 2.06x105 | 792 | 6.268 x10-6 | 48.73 |
| - | - | - | av.(de/dN) = 6.9x10-6 | av.ΔS = 46.9 |

Table 6. Calculations for crack growth in water-quenched steel and references at (475 °C)

| bo= 0.195 | b1= 4.27 x 10-6 | | b2 =5.56 x 10-12 | |
|---|---|---|---|---|
| a (mm) | Nf (cycle) | $\sigma$ (N/mm2) | de/dN (mm/cycle) | $\Delta S$ $(MPa.m^{1/2})$ |
| 0.66 | 1.31x105 | 602 | 3.555 x10-6 | 26.97 |
| 0.81 | 1.79x105 | 573 | 3.284 x10-6 | 28.82 |
| 0.84 | 2.003x105 | 552 | 3.128 x10-6 | 27.93 |
| 1.04 | 3.77x105 | 543 | 2.179 x10-6 | 30.44 |
| - | - | - | av.(de/dN) = 3.04x10-6 | av. $\Delta S = 28.6$ |

Table 7. Calculations for crack growth in water-quenched steel and references at 675C°

| bo= 0.65 | b1= 2.42 x 10-6 | | b2 =1.13x 10-12 | |
|---|---|---|---|---|
| a (mm) | Nf (cycle) | $\sigma$ (N/mm2) | de/dN (mm/cycle) | $\Delta S$ $(MPa.m^{1/2})$ |
| 0.763 | 5.62x104 | 503 | 2.344 x10-6 | 24.47 |
| 1.05 | 1.75x105 | 452 | 2.214 x10-6 | 25.73 |
| 1.45 | 4.24x105 | 404 | 1.937 x10-6 | 26.92 |
| 1.63 | 5.39x105 | 382 | 1.81 x10-6 | 27.12 |
| - | - | - | av.(de/dN)=2.077x10-6 | $av.\Delta S$ =26.06 |

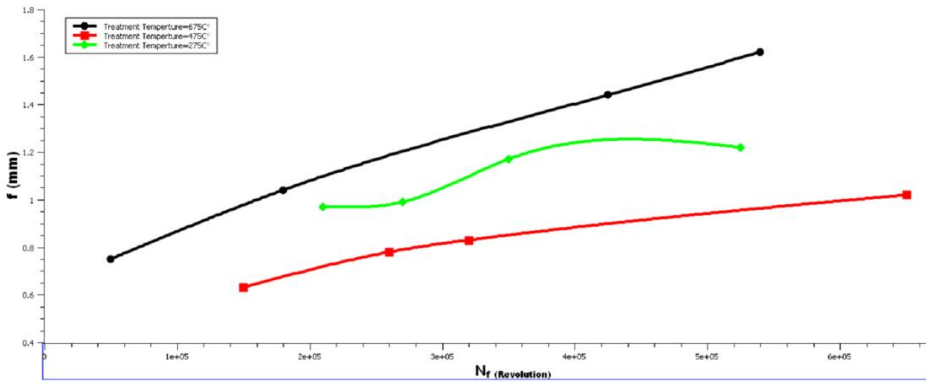


Fig. 7. Relationship between notch length and number of cycles for AISI 1045 steel tempered in water and referenced at temperatures of 275, 475, and 675 °C

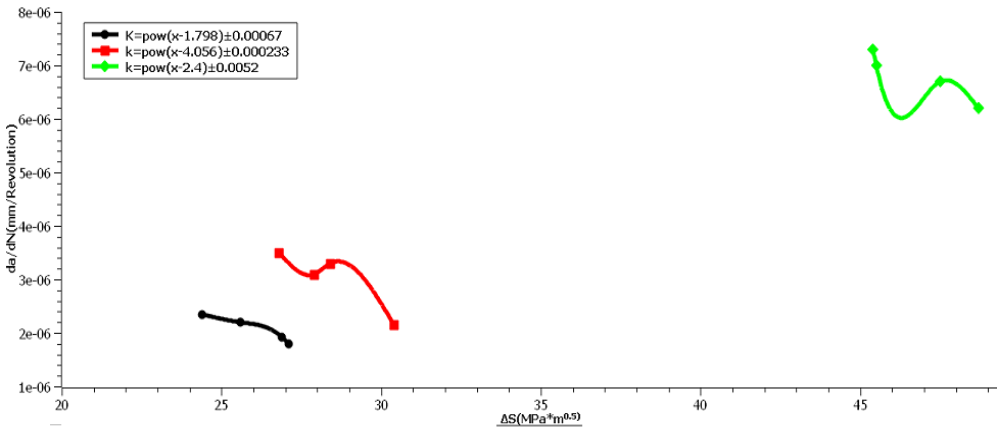


Fig. 8. Relationship between notch propagation velocity and stress intensity for medium carbon steel quenched in water and referenced at temperatures of 275, 475, and 675 °C

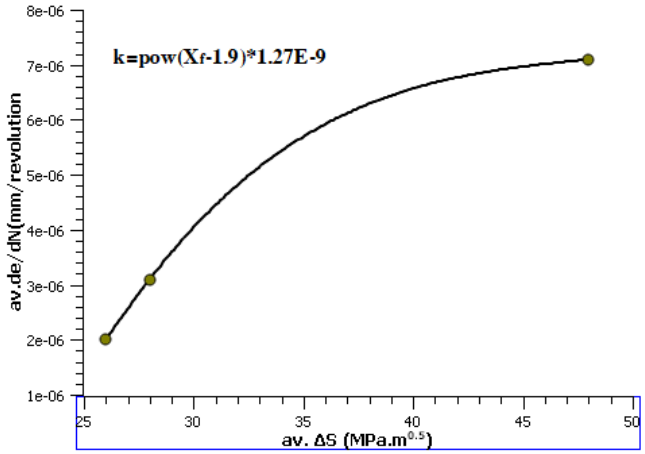


Fig. 9. Relationship between the crack propagation rate and the stress intensity factor for medium-carbon steel quenched in water and referenced at temperatures of (275, 475, 675 ºC)

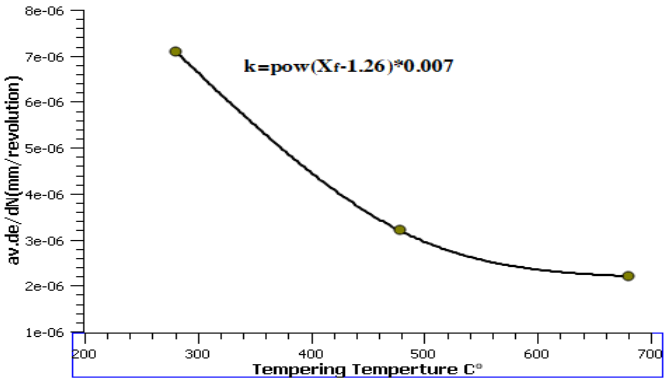


Fig. 10. Relationship between notch propagation rate and stress intensity factor for medium carbon steel quenched in water and referenced at temperatures of 275, 475, 675ºC

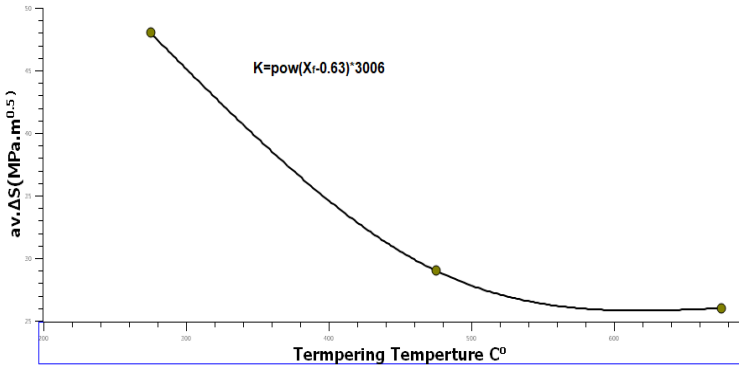


Fig. 11. Relationship between the notch propagation rate and the reference temperature for medium-carbon steel tempered in water and referenced at temperatures of ( 275, 475, and 675ºC)

### 3.1. THE EFFECT OF HARDENING ON FATIGUE RESISTANCE

Fatigue often occurs through the formation of slip bands, so any treatment that increases hardness or resistance to yielding and tension will increase the level of stress required for slippage, which in turn increases fatigue resistance. This is clearly evident in water-hardened

samples, which showed an increase in fatigue limit (742 MPa), i.e., a 131.5% improvement in fatigue limit compared to the base metal consisting of ferrite and pearlite, which had a fatigue limit of 323 MPa. As for the oil medium, it gave a lower fatigue resistance than the water medium, reaching (472 MPa), meaning that the improvement in fatigue limit was (47.5%) compared to the base metal. This is because the cooling rate in oil is lower than the critical cooling rate.

### 3.2. EFFECT OF THE REVIEW PROCESS ON FATIGUE RESISTANCE

The review temperature of 275ºC o gave the highest fatigue resistance relative to the water medium. This is attributed to the elimination of internal stresses resulting from the hardening process, as well as the formation of a martensite structure with a small amount of bainite, where the fatigue limit for this structure increased to (782M Pa) despite a high slope in the stress-cycle curve, i.e., failure occurred after a few cycles for the applied stress values, especially at high stresses close to the yield stress, because the plastic energy required for failure is relatively high, so the fatigue life is short. where the crack growth rate increases significantly at this stage, increasing its critical length and thus causing final fracture after a few cycles of crack formation.

As for the oil medium at the same temperature, the fatigue limit increased to (523 MPa) compared to the metal hardened in oil, due to the formation of a small amount of bainite with ferrite and pearlite.

The review temperature of 475 ºC gave lower fatigue resistance than the hardened metal for both media, with a fatigue limit of 522 MPa for water as a hardening medium and 443 MPa for oil as a hardening medium due to an increase in grain size and a decrease in residual compressive stresses.

The review temperature of 675 ºC led to a decrease in fatigue resistance for both media until it became close to that of the base metal due to cementite coarsening, i.e., the formation of a spherical pearlite structure and the removal of residual stresses. The stress-cycle curves for oil-hardened steel and reference steel at different temperatures were compared with the base metal and with water. The fatigue lives for different tempering temperatures were also compared by plotting curves.

## 4. CONCLUSIONS

The highest hardness obtained for hardened steel and references relative to water and oil media is at a reference temperature of 275 ºC.

A tempering temperature of 475 ºC for the water medium gave the optimum properties for AISI 1045 steel in terms of hardness, impact resistance, and fatigue.

Increasing the tempering temperature led to a change in the type of fracture from brittle fracture to ductile fracture.

Quenching in water followed by tempering at 275 ºC improved fatigue resistance, with an improvement of 144.5% compared to the base metal.

Mathematical relationships linking fatigue resistance, tensile strength, and hardness were established.

The mathematical model based on the stress intensity factor in calculating fatigue life showed greater accuracy than the model based on crack propagation rate (de/dN). Both models gave fatigue lives lower than the practical value, which provides a good safety factor for the designer.

The treatment involving water quenching and tempering at 275$^{o}$C proved to be important in low-cycle fatigue applications, i.e., at less than 107 revolution.

## REFERENCES


[1] PATOKAR P., TRIKAL S.P., PATIL CH., 2016, *Experimental Investigation of Machining Time in Turning Mild Steel Component Using Multi Tool Turning Method*, IJSRD - International Journal for Scientific Research & Development, 3/11, 2321–0613.

[2] OBAID S.H., JABER J.A., IBRAHIM H.R, 2019, *Studies on the Steel Reinforcement Performance in Presence of Nacl: Effects of Salt Concentration and Temperature*, IOP Conf. Series: Materials Science and Engineering, 557, 012078, https://doi.org/10.1088/1757-899X/557/1/012078.

[3] HERMANIUK T., 2021, *Automation of Production Processes as an Element of Improvement of the Products' Quality*, QPI, 3, 339–347, https://doi.org/10.2478/cqpi-2021-0033.

[4] NAGIE J.M,, 2014, *The Effect of Cooling Rate on Mechanical Properties of Carbon Steel (St 35)*, Diyala Journal of Engineering Sciences, 07/01, 109–118.

[5] IBRAHIM H.R., ALBAKRI R.A., HATAMOBAID S., 2020, *Experimental and Theoretical Study of Shearing Angles and Cutting Speed Effects on Dynamic Cutting Forces in Punch-Die System*, Technology Reports of Kansai University, 62/3, 45–51.

[6] BARRAZA-FIERRO J., CAMPILLO-ILLANES B., XIMING LI, CASTANEDA H., 2018, *Steel Microstructure Effect on Mechanical Properties and Corrosion Behavior of High Strength Low Carbon Steel*, Metallurgical and Materials Transactions A, 45A, 2014–3981.

[7] SUNG H.K., LEE D.H., LEE S., LEE B., HONG S., KIM Y., 2017, *Effects of C and Si on Strain Aging of Strain-Based API X60 Pipeline Steels*, MMI, 23, 450–458, https://doi.org/10.1007/s12540-017-6457-7.

[8] SUNG H.K., LEE D.H., LEE S., LEE B.J., HONG S.P., KIM Y.W., YOO J.Y, HWANG B., SHIN S.Y., 2017, *Effects of C and Si on strain aging of strain-based API X60 pipeline steels*, Metals and Materials International, 23, 450–458.

[9] ALAR Z., MANDI D., 2018, *Comparison of Impact and Tensile Properties of High-Strength Steel*, Metals, 8/7, 511, https://doi.org/10.3390/met8070511.

[10] AL-SULTAN M.J., AL-RIFAI A., 2024, *Numerical Study on the Impact Response of Steel Beams with Large Web Openings: Investigating Key Parameters*, Mathematical Modelling of Engineering Problems, 11/3, 619–630.

[11] BREESEM K.M., OBAID S.H., JABER J.A., 2024, *Experimental and Numerical Investigations of the Crack Angle Effect on the Shaft Strength Due to Torsional Loading*, Electromechanical Engineering and its Applications AIP Conf. Proc. 3002, 080003-1-080003-9, https://doi.org/10.1063/5.0205715.

[12] CHAOUCH D., SADOK A., BENDAOUDI S-E., CHAOUCHA B., 2018, *Effect of Charpy Impact Test on Microstructure Properties of AISI4140 Steel*, Mechanics and Mechanical Engineering, 22/4, 1463–1469, https://doi.org/10.2478/mme-2018-0114.